Roll-to-roll dip coating of three different PIMs for Organic Solvent Nanofiltration

Marcus Cook, Piers R.J. Gaffney, Ludmila G. Peeva, Andrew G. Livingston

www.elsevier.com/locate/memsci

PII: S0376-7388(18)30568-4
DOI: https://doi.org/10.1016/j.memsci.2018.04.046
Reference: MEMSCI16130

To appear in: *Journal of Membrane Science*

Received date: 1 March 2018
Revised date: 23 April 2018
Accepted date: 26 April 2018

Cite this article as: Marcus Cook, Piers R.J. Gaffney, Ludmila G. Peeva and Andrew G. Livingston, Roll-to-roll dip coating of three different PIMs for Organic Solvent Nanofiltration, *Journal of Membrane Science,* https://doi.org/10.1016/j.memsci.2018.04.046

Roll-to-roll dip coating of three different PIMs for Organic Solvent Nanofiltration

Marcus Cook, Piers R.J. Gaffney, Ludmila G. Peeva, Andrew G. Livingston*

Barrer Centre, Department of Chemical Engineering, Imperial College London, SW7 2AZ, UK

*email: a.livingston@imperial.ac.uk

Abstract

PIM-1, PIM-7, and PIM-8 composite membranes have been fabricated for Organic Solvent Nanofiltration (OSN) on two different support membranes. Both support membranes, PAN and crosslinked Ultem 1000, displayed pore sizes within the range of 20 – 25 nm as characterised by gas liquid porometry. PIM layers of <500 nm thickness were formed from dip coating on a roll-to-roll pilot line. The resultant composite membranes exhibited typical MWCOs in the region of 500-800 g mol^{-1}. The quality of coating obtained on the crosslinked Ultem 1000 support membrane was consistently higher for all three PIMs than that obtained on the PAN membrane. The PIM composite membranes coated on to crosslinked Ultem 1000 were stable in a wider range of solvents than those on the PAN support. OSN testing in a model system with isomeric alkane solutes verified that manipulated changes to the molecular architecture of the polymer backbone resulted in a higher *separation factor between straight and branched alkane isomers*.

Keywords: Organic Solvent Nanofiltration; Thin film composite membrane; Dip coating; Polymer of Intrinsic Microporosity

1 Introduction

Polymers of Intrinsic Microporosity (PIMs) are an attractive class of materials for separation processes. A favorable characteristic of the PIMs is that they are solution processable polymers with highly rigid, contorted structures that frustrate the polymer packing upon drying, giving rise to a continuous network of intermolecular voids that are <2 nm in dimension [1]. PIMs may enable expansion of the current gas separation applications [2], and have potential applications in OSN [3]. More than a decade since the *invention of PIMs*, PIM-1 remains one of the most researched and most promising materials from this class of polymers. Various reports detail efforts to understand and optimise the synthesis and purification of PIM-1 to produce a higher quality polymer [4–7]. Self polymerisation of an AB-type monomer is also a promising route to obtaining high molecular weight PIM-1 [8]. Alternative PIMs are typically synthesised from monomers that require custom synthesis, and their polymerisation conditions and purification protocols are less optimised than those of PIM-1.

Bench scale dip coating of PIM-1 onto PVDF supports enabled thicknesses down to 1 µm to be achieved for pervaporation [9]. Coatings were applied to PVDF membranes of different pore sizes, and no significant change to the thicknesses of the obtained PIM-1 layer were reported. Adhesion of PIM-1 to PVDF support membranes, however, has been reported to be problematic for OSN [10]. There have also been problems reported for adhesion between PIM-1 and PAN, such that an epoxy resin based crosslinking procedure within the PIM-1 material was needed to enable filtrations in aromatic solvents [11]. Without this crosslinking, there were reports of partial

detachment of PIM-1 in toluene and acetone. The crosslinking procedure, however, rendered the membranes unsuitable for alkane solvents. When a gutter layer was used to prevent problems associated with coating on to a porous substrate, PIM-1 composite membranes with higher solvent fluxes and lower rejections were obtained [11].

In attempts to either increase the stability or tune the molecular separation properties of PIM based polymers, various wet phase chemical techniques are detailed throughout the literature. These include the synthesis of alternative PIMs [12–15], and blending of PIMs with other polymers [16]. Wet chemical routes can introduce challenges such as: changing the solution properties of the final polymer, interference with the porous structure of a native unmodified PIM when blending in additives, and in some cases health and safety considerations from the use of hazardous chemicals. There is also the limitation that only a few monomers are capable of reacting to give sufficiently high molecular weight [2]. The synthesis of PIM co-polymers is typically conducted via one-pot co-polymerisation [17–19]. As properties of a co-polymer are controlled by their monomer sequence distribution along the chain, which is in turn dependent upon polymerisation conditions, alternative strategies to synthesise perfectly alternating PIM co-polymers through the use of an ABA trimer intermediate have been researched [20]. Along with this strategy, the phenazine route to synthesise PIMs is one which has received less attention, but which does allow for the fabrication of a homopolymer rather than a random co-polymer [13,14]. This approach is used within the present research.

Post treatments of PIM membranes such as thermal annealing [21,22], chemical treatment and crosslinking [23–25], or UV exposure [26–28] have also been studied. The temperatures required to induce thermal oxidation of the PIM-1, and apparently crosslink the polymer, are beyond those achievable on composite flat sheet polymer membranes, whilst prolonged exposure to UV radiation degrades PIM-1 [28]. The majority of the reported PIM research is on powders or thick films (>30 μm); the evaluation of which is only one small part of the membrane development [29]. The influence of the support membrane on the fabrication of a composite membrane is one that does not receive much attention in the PIM literature, but is a crucial factor in determining the usability of the final composite membrane. In part, this is due to the limited number of suitable polymer ultrafiltration membranes with chemical stability capable of withstanding dip coating using solvents in which PIM is soluble.

Other than PIM-1, there are no reports of applications of other PIMs in OSN. It has been reported that the PIM-7 and PIM-8 polymers have a stronger bias towards sub-nanometer pores than the PIM-1, on the basis of nitrogen adsorption experiments. [13]. We therefore decided to investigate whether these measurements translated to composite membrane performance, and if manipulation of the molecular architecture along the polymer backbone could create membranes with lower Molecular Weight Cut Off (MWCO). Although other PIMs are available which display similar bias in pore size, the synthesis of these two PIMs is relatively practical. As TFC membranes are required to study solvent nanofiltration, the feasibility of thin film composite manufacture of PIMs is therefore also explored. Three variants of PIM (PIM-1, PIM-7, and PIM-8) coated on two different support membranes (PAN, and a crosslinked polyetherimide) were produced during roll-to-roll coating trials. Uniform coating layers *of* 200 - 300 nm *thicknesses* were achieved from continuous dip coating. OSN testing with isomeric alkane solute markers verified that the *PIM-8 exhibited a higher separation factor between alkane isomers then the other variants, suggesting a tighter polymer network.*

2 Methods

2.1 Materials

Unless stated otherwise, solvents were of reagent grade and were obtained from VWR, along with sulfuric acid (95%) and potassium carbonate. 1,3-Dioxolane (anhydrous) was obtained from Sigma Aldrich. *Unless stated, chloroform stabilised with ethanol (0.6 wt % EtOH) from VWR was used. Otherwise, amylene stabilised chloroform (anhydrous, ≥99%) obtained from Sigma Aldrich was used*. Tetrafluoroterephthalonitrile/1,4-dicyanotetrafluorobenzene (DCTB, 99%) was obtained from Fluorochem. Cerium (IV) ammonium nitrate (REacton, 99.5%) and 4,5-dichloro-*o*-phenylenediamine (98%) were obtained from Alfa Aesar. 2,5-Hexanedione (synthesis grade) was obtained from Sigma Millipore. 1,2-Dihydroxybenzene was obtained from Acros Organics. *n*-Hexadecane (99%) and 2,2,4,4,6,8,8-heptamethylnonane (*i*-hexadecane, 98%) were obtained from Sigma Aldrich. 1,3-Diaminopropane (≥99%) and 18-crown-6 (99%) were obtained from Sigma Aldrich. Polyacrylonitrile (PAN, 230k) was obtained from Goodfellow. Ultem 1000 was obtained from Resinex. Commercially available PDMS based membranes Evonik Selective and oNf-2 were obtained from Evonik and GMT respectively.

2.2 Synthesis procedures

5,5',6,6'-Tetrahydroxy-3,3,3',3'-tetramethyl-1,1'-spirobisindane (TTSBI, >97%, Alfa Aesar), was recrystallized from methanol-CH_2Cl_2. 4,5-Dichlorobenzene-1,2-diamine (Alfa Aesar, 98%) and all other reagents were used as received. All monomers and reagents were dried in a vacuum oven at 120°C overnight prior to polymerisation reactions. All glassware was dried in a convection oven at 100°C, then purged with argon before addition of reagents. All reactions were conducted under an argon atmosphere. All polymerisation reactions were run in DMF dried over 4Å molecular sieves (Sigma Aldrich).

2.2.1 Synthesis of monomers

2.2.1.1 Bisquinone of TTSBI (O-TTSBI)

To MeCN-water (3:1 v/v, 1 L) were added TTSBI (10.0 g, 29.4 mmol), then ceric ammonium nitrate (65 g, 119 mmol, 4.05 eq.), and the mixture was stirred for 3 hours at room temperature. MeCN was then removed by rotatory evaporation (water bath 35°C, until the pressure fell to 20 mbar). Brine (250 mL) was added to the residual aqueous solution, which was extracted with chloroform (300 mL). The chloroform was evaporated, and the residue (11.72 g) was washed with water, then dried under vacuum. The crude product was crystallised from glacial acetic acid to yield the title compound as a red solid (6.54 g, 56%).

R_f (MeOH-$CHCl_3$ 1:19) TTSBI 0.30; O-TTSBI 0.53

^{1}H NMR (400 MHz, $CDCl_3$) δ 6.29 (d, *J* = 0.7 Hz, 2H), 6.19 (d, *J* = 0.8 Hz, 2H), 2.40 (d, *J* = 13.5 Hz, 2H), 2.26 (d, *J* = 13.4 Hz, 2H), 1.43 (s, 6H), 1.41 (s, 6H).

^{13}C NMR (101 MHz, $CDCl_3$) δ 178.40 (C), 178.34 (C), 167.81 (C), 167.00 (C), 124.93 (CH), 122.00 (CH), 56.59 (CH_2), 54.79 (C), 43.10 (C), 30.30 (CH_3), 28.58 (CH_3).

2.2.1.2 Tetrachloro Monomer

To glacial acetic acid (600 mL) were added 4,5-dichlorobenzene-1,2-diamine (7.08 g, 40 mmol, 2.08 eq.), then O-TTSBI (6.44 g, 19.2 mmol). The mixture was refluxed for 3 hours. The mixture was then cooled, the crude product collected by filtration and washed with glacial acetic

acid, boiling water, and ethanol. The brown/yellow powder was dried under vacuum at 120°C overnight to return the title compound (10.72 g, 81%).

R_f (MeOH-$CHCl_3$ 1:19) O-TTSBI 0.53; Cl_4 monomer 0.88

^{1}H NMR (400 MHz, $CDCl_3$) δ 8.37 (s, 2H), 8.22 (s, 2H), 8.08 (s, 2H), 7.68 (s, 2H), 2.75 (d, *J* = 13.2 Hz, 2H), 2.70 (d, *J* = 13.2 Hz, 2H), 1.71 (s, 6H), 1.63 (s, 6H).

^{13}C NMR (101 MHz, $CDCl_3$) δ 158.70 (C), 158.27 (C), 143.97 (C), 143.93 (C), 141.46 (C), 141.28 (C), 135.05 (C), 134.92 (C), 129.64 (CH), 129.60 (CH), 124.37 (CH), 121.53 (CH), 59.84 (CH_2), 57.39 (C), 44.14 (C), 31.96 (CH_3), 30.24 (CH_3).

2.2.1.3 2,3,6,7-Tetrahy-droxy-9,10-dimethyl-9,10-ethanoanthracene

To a stirred solution of catechol (100 g, 0.91 mol) in 70% H_2SO_4 (1 L) was slowly added 2,5 hexanedione (27.7 mL, 0.24 mol) dropwise from a dropping funnel over a duration of 30 min. After addition, the dark brown reaction mixture was left to stand for a week at room temperature during which time crystals slowly formed. The mixture was then diluted with water (1.5 L), filtered, and the obtained solids washed with water. After drying in a vacuum oven overnight at 120°C, the crude material (39.5 g) was crystallised from ethanol to give the title compound as white crystals (13.9 g, 17.6%).

^{1}H NMR (400 MHz, CD_3OD) δ 6.72 (s, 4H), 1.78 (s, 6H), 1.49 (s, 4H).

^{13}C NMR (101 MHz, CD_3OD) δ 141.50 (C), 138.59 (C), 108.17 (CH), 40.19 (C), 36.41 (CH_2), 17.77 (CH_3).

2.2.2 Synthesis of PIM-1

A solution of TTSBI (10.2 g, 30 mmol) and DCTB (6.0 g, 30 mmol) in anhydrous DMF (200 mL) was warmed to 65°C. To the solution was added K_2CO_3 (8.5 g, 61.2 mmol) and the reaction mixture was stirred at 65°C for 2 days. After cooling, the mixture was poured into water (300 mL). The solids were collected by filtration and washed with water then methanol, and dried in a vacuum oven at 120°C overnight. The resultant yellow powder (13.3 g) was dissolved in chloroform, filtered, and re-precipitated from methanol to give PIM-1 (8.9 g, 67%, Mw = 70,000, PDI = 1.39).

2.2.3 Synthesis of PIM-7

To a solution of TTSBI (4.77 g, 14 mmol), the tetrachloro monomer (8.67 g, 14 mmol) and 18-crown-6 (3.71 g, 14 mmol) in anhydrous DMF (400 mL), was added K_2CO_3 (11.56 g, 84 mmol). The reaction mixture was stirred at 155°C for 3 days. After cooling, the mixture was poured into stirred 1 vol % HCl (2 L). The solids were collected by filtration and washed with water, methanol, and toluene then dried in a vacuum oven at 120°C overnight. The crude orange powder (11.56 g) was dissolved in chloroform, filtered, and subjected to two re-precipitations, first from methanol (9.86 g), and then from THF, to yield PIM-7 (6.27 g, 47%) as a yellow/orange powder.

2.2.4 Synthesis of PIM-8

The synthesis of PIM-8 was similar to that of the PIM-7. To a solution of 2,3,6,7-tetrahy-droxy-9,10-dimethyl-9,10-ethanoanthracene (4.92 g, 16.5 mmol), tetrachloro monomer (10.20 g, 16.5 mmol) and 18-crown-6 (4.36 g, 16.5 mmol) in anhydrous DMF (400 mL) at 155°C, was added K_2CO_3 (13.20 g, 95.6 mmol). The reaction mixture was stirred at 155°C for 3 days. After

cooling, the mixture was poured into stirred 1 wt % HCl (2 L). The solids were collected by filtration and washed with water, methanol, and toluene, and then dried in a vacuum oven at 120°C overnight. The crude polymer (12.8 g) was dissolved in chloroform, filtered, and subjected to two re-precipitations, first from methanol (10.42 g), and then from THF, to yield PIM-8 (9.18 g, 61.9%) as a yellow/orange powder.

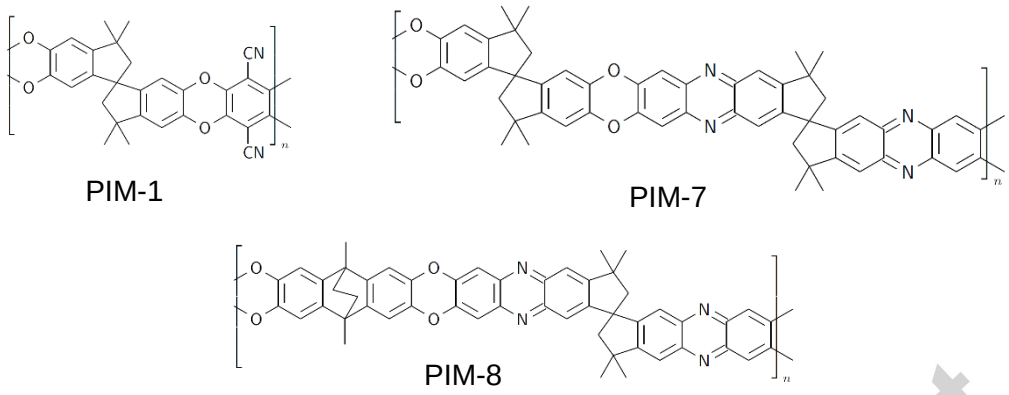

Fig. 1. Chemical structures of PIM-1, PIM-7, and PIM-8.

2.3 Membrane preparation

2.3.1 Fabrication of support membranes

A polyacrylonitrile (PAN) ultrafiltration membrane was prepared from a polymer solution of PAN:DMSO:1,3-dioxolane at a w/w ratio of 22:89:89. This mixture was heated overnight at 75°C. Upon cooling the polymer solution was subject to two filtration steps: firstly through a 41 micron filter (NY4104700, Merck), and subsequently through an 11 micron filter (NY1104700, Merck) using a nitrogen pressurised filtration cell (XX4004740, Merck) at pressures of up to 70 psi. The resultant polymer solution had a viscosity of 20,000 cP. The membrane was cast on to a PET non-woven *fabric* (Hirose RO grade) on a continuous casting machine (SepraTek, South Korea) with a web width of 0.3 m. Immediately after casting, the membrane was immersed in water at a temperature of 80°C for 3 hours [30], and after cooling, dried from water, IPA, or heptane. This procedure led to reproducible support membranes with pore sizes in the range of 20 – 25 nm as characterised by capillary flow porometry (Porolux 1000, Porometer), with typical heptane permeances of several hundred l m^{-2} h^{-1} bar^{-1}.

A solvent stable ultrafiltration membrane from Ultem 1000 was prepared by dissolving the polymer in a 50:50 mixture of DMSO:1,4-dioxane at 15 wt %. The powder dissolved readily and was cast on to the *same PET non-woven fabric* (Hirose RO grade) at a web speed of 8 m min^{-1}. The roll of membrane was collected, and after storage in water was transferred to IPA. The roll was then placed into a reactor vessel with IPA (10 L), and propanediamine was added to the vessel at 0.44 vol %. The vessel was then heated to 60°C by means of a heated jacket and left for 4 hours. The resulting crosslinked membrane was then cooled and washed with IPA, and further air dried.

2.3.2 Dip coating of PIMs

A solution of PIM was prepared by dissolving the polymer at either 0.6 or 1.0 wt % in $CHCl_3$. The solution was then filtered through an 0.2 µm PTFE filter (FGLP04700, Merck) and allowed to degas. For the PIM-7 and 8, there was a requirement that a trace quantity of alcohol was present in the chloroform to allow for polymer dissolution. When attempting to dissolve *these*

two PIMs in $CHCl_3$ (200 ppm amylene stabilised), aggregates of undissolved polymer were observed. Upon the addition of 1 - 2 parts of alcohol per 100 parts $CHCl_3$, a clear solution was obtained. The influence of using both methanol and ethanol as co-solvents in the coating solution were studied. The coatings were conducted on a roll-to-roll pilot line *(RK Print, UK)* with a web width of 30 cm. Typically, a web speed of 5 m min^{-1} was used, with three air convection dryers in series set at incremental temperatures of 30, 35, and 40°C. Each dryer was of length 1 meter. A schematic of the coating line can be seen in Fig. 2.

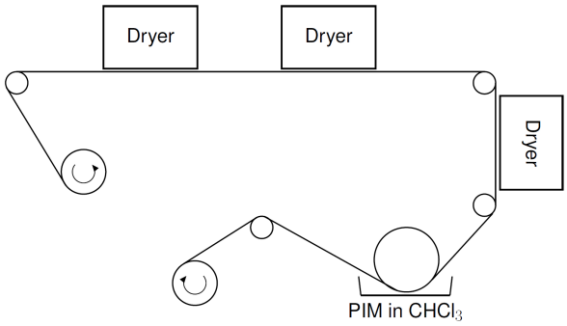

Fig. 2. Schematic diagram of roll-to-roll dip coating line.

2.4 Membrane characterisation

2.4.1 Molecular weight characterisation

GPC was conducted using a multi-detector gel permeation chromatography (1260 Infinity GPC system with 1260 RID and DAD VL attachments, Agilent Technologies). Chlorobenzene *(Analytical grade)* was used as the eluent, and the measurements were performed at 80°C using two PL gel 10 µm MIXED B columns in series. A GPC flowrate of 1 mL min^{-1}, along with an injection volume of 50 µL were used. Calibration of the molar mass against elution time was conducted using Agilent EasiVial narrow dispersity polystyrene standards. The elution time of the PIM-1 was compared to these standards to estimate the MW. *The requirement for addition of a trace of alcohol within chlorobenzene to form clear solutions of PIM-7 and PIM-8* prevented characterisation via GPC. *Therefore,* Ubbelohde viscometers (Universal size OC, Cole Palmer UK) were used to estimate the intrinsic viscosity of the polymer solutions. Dilute solutions of the PIM were prepared in chloroform, and the time taken for the solution to pass through the viscometer at 25°C was recorded. Extrapolation of the reduced viscosity plotted against concentration enabled an estimate of the intrinsic viscosity; further details are in Supplementary Information, Section S2.

2.4.2 Intelligent Gravimetric Analysis (IGA)

Solvent vapour sorption experiments were conducted using an Intelligent Gravimetric Analyser (IGA-002, Hiden Isochema, UK). The analysis was conducted on free standing films of PIM with thicknesses of 25 - 50 µm. *For this purpose, thick free standing films were fabricated via solvent evaporation to enable characterisation via vapour sorption analysis. Typically, a 3 wt \% solution of the PIM polymer was dissolved in chloroform, and filtered through an 0.2 µm PTFE syringe filter on to a glass petri dish purged with argon*. *The films of PIM-7 and PIM-8, however, were too brittle to be used as free standing membranes*. Prior to each new isotherm, the PIM was heated to 120°C under an ultra-high vacuum environment (10^{-7} mbar) until the sample mass was constant, to ensure residual solvent from previous experiments was removed. Typically, a minimum of 1 hour was given at each pressure change within the isotherm experiment to ensure a steady state was reached. The vapour pressure of each of the solvents studied was calculated at the operating temperature using the Antoine equation.

2.4.3 Porometry

Pore size measurements of the support membrane were conducted using capillary flow porometry with a Porolux™ 1000. Membrane samples were immersed in the Porefil wetting liquid (16 dyn cm^{-1} surface tension) for a minimum of 15 minutes prior to analysis.

2.4.4 Attenuated total reflectance Fourier Transform Infrared Spectroscopy (ATR-FTIR)

ATR-FTIR spectra were recorded on a Perkin-Elmer Spectrum 100 spectrometer between wavenumbers of 4000–600 cm^{-1}. The instrument was equipped with a Universal ATR sampling accessory (diamond crystal), with a red laser excitation source (633 nm), and a middle infrared (MIR) triglycine sulphate (TGS) detector.

2.4.5 Atomic Force Microscopy (AFM)

AFM was conducted using a Multimode 8 (Bruker, USA) equipped with a vertical engage J scanner. Peak force tapping was conducted on membrane samples stuck on a magnetic disc using ScanAsyst in air with MSNL-10 probes with nominal spring constant of 0.6 N m^{-1}.

2.4.6 Scanning Electron Microscopy (SEM)

Membrane samples were freeze fractured in liquid nitrogen to obtain images of the cross section. Prior to imaging, the samples were coated with chromium using an Emitech K575X Peltier. SEM images were obtained with a high resolution LEO1525 Karl Zeiss SEM at an accelerating voltage of 5 kV.

2.4.7 Light Microscopy

Surface images were obtained via light microscopy using a Keyence VHX-900F, with a VH-Z100R lens.

2.5 OSN performance

Composite membrane performance was obtained in a cross flow filtration set up comprising two lines, each containing 4 membrane cells in series, enabling a total of 8 membranes to be tested [31]. The active membrane area of each cell was 14 cm^2, and the pump speed was set to provide a cross flow rate of 1 L min^{-1}. Unless otherwise stated, a Transmembrane Pressure (TMP) of 30 bar was applied. The MWCO curves were obtained using polystyrene standards dissolved in either heptane or toluene [32]. The styrene oligomer mix contained 1 g L^{-1} each of PS 580 and PS 1100 (Agilent) along with 0.1 g L^{-1} of α-methylstyrene dimer (Sigma-Aldrich, UK), and was analysed using an Agilent HPLC system with a UV/vis detector set at 264 nm. Prior to analysis, solvent swaps were performed from both toluene and heptane to acetonitrile. Separation of the oligomers was achieved using a reverse phase column (C18-300, 250 x 4.6 mm), with a mobile phase consisting of 90 vol% methanol and 10 vol% THF, operating at a flow rate of 1 mL min^{-1}. A minimum of 4 repeat membrane samples were used, and as such the standard deviations reported later represent the standard deviation of the mean of these samples. Rejection of each oligomer was calculated from the following equation:

$$R_i = \left(1 - \frac{C_{p,i}}{C_{F,i}}\right) x\ 100 \quad (1)$$

where $C_{p,i}$ and $C_{F,i}$ correspond the concentrations of each polystyrene oligomer in the permeate and feed respectively. Additional OSN characterisation was conducted using

hexadecane isomers as marker solutes in heptane. In this case, the feed solution comprised of 99 wt % heptane, along with n and i-C_{16} each at 0.5 wt %. Analysis of this mixture was conducted by GC-FID (Agilent, 6850) using a HP-5 column (19095J-323E, Agilent). The column temperature was ramped at 15°C min^{-1} from 40°C to 220°C. The rejection was calculated in the same methodology as above. For analysis using the hexadecane isomers, the performance of each membrane disc (14 cm^2) is reported individually. In all filtration experiments, the stage cut was low (<0.05).

3 Results and discussion

3.1 Polymer synthesis

The monomers required for the PIM-7 and PIM-8 were synthesised with high purity, as shown in the ^{1}H NMR and ^{13}C NMR spectrum in Supplementary Information, Section S1. Cerium Ammonium Nitrate proved an efficient oxidizing agent for the TTSBI, returning a yield of 56% after a crystallisation step. The PIM-1 was synthesised using optimised reaction conditions previously reported in the literature [5], and was characterised by GPC as having a MW of 70,000 with a polydispersity index of 1.39 when compared to polystyrene standards with chlorobenzene as solvent. The intrinsic viscosity of the PIM-1 was found to be in the region of 55 – 60 mL g^{-1}. GPC analysis of PIM-7 and PIM-8 proved problematic due to solubility issues. Intrinsic viscosities of these two polymers were calculated to be 25 – 30 mL g^{-1} and 20 – 25 mL g^{-1} respectively. Initial characterisation of the PIMs was conducted via vapour sorption analysis to assess differences between the PIMs, and whether this translates into their performance as SRNF membranes.

3.1.1 Vapour sorption isotherms

Vapour sorption isotherms of the three different PIMs were obtained via an Intelligent Gravimetric Analyser (IGA). *The isotherms are of* a dual mode uptake profile, characteristic of vapour sorption into glassy polymers, as shown in Fig. 3. Two sample *sample sorption/desorption datasets* obtained from the IGA apparatus are shown in Supplementary Information, Section S3. Attempts at swelling *thick*, free standing films of the PIMs into organic solvents proved difficult and erroneous. This was particularly true for PIM-7 and PIM-8, for which free standing films *became brittle upon drying and impossible to handle*. It has been shown that swelling a free standing film in the liquid phase corresponds to the vapour phase uptake [33]. Therefore, it was chosen to study the vapour phase uptake through gravimetric analysis of the free standing films. Typical film thicknesses were in the 25 – 50 µm range as gauged by a micrometre.

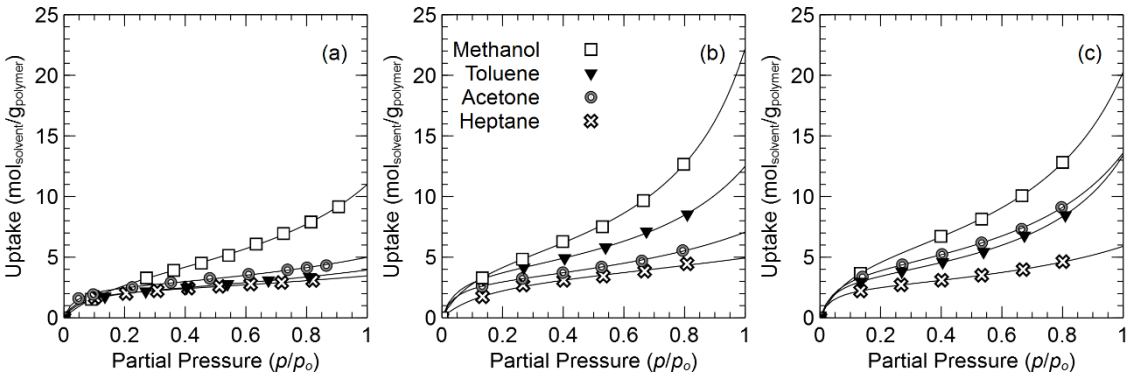

Fig. 3. Vapour sorption isotherms of various solvents into (a) PIM-1, (b) PIM-7, and (c) PIM-8 at 30°C on a molar basis. Solid lines are regressed fits of the GAB model.

Detailed analysis of vapour sorption isotherms for PIM-1 can be found elsewhere in the literature [34]. Within that study, *all the sorption isotherms of organic vapours were of type 2 (S shape) and were successfully fitted* using a layered adsorption model developed by Guggenheim, Anderson and de Boer (GAB). It was one purpose of our research to compare the solvent vapour sorption uptake profiles of the alternative PIMs (7 and 8) with that of PIM-1, and investigate any correlation to the OSN performance. Since a previous paper [34] details the application of the GAB model to PIM-1, we decided, for consistency, to apply that same model here to the three different in-house synthesised PIMs. The GAB model is an extension of BET theory developed under the assumption that all sorption sites are the same, but that the species absorbed in the first monolayer have a different thermodynamic state to those adsorbed in higher layers. This introduces a third *fitting* parameter, and the GAB theory is described by:

$$\boldsymbol{c} = \frac{\boldsymbol{v_m h f a}}{(\boldsymbol{1-fa})(\boldsymbol{1-fa+hfa})} \qquad (2)$$

where v_m is the GAB monolayer capacity, h is a dimensionless parameter related to the heat of adsorption of the monolayer, f is a dimensionless parameter related to the heat of adsorption in the multilayer region, and the activity, $\boldsymbol{a}$, is defined as $a = p/p^{sat}$, with p and p^{sat} the actual and saturated vapour pressure, respectively.

Table 1. Parameters of the GAB sorption model (Eq. 2) obtained using a least squares minimisation method, along with the corresponding Residual Sum of Squares (RSS).

Polymer	Solvent	v_m (mmol g^{-1})	f	h	RSS
PIM-1	Toluene[1]	2.75	0.69	23.0	
	Toluene	2.31	0.43	39.8	0.031
	Acetone	2.65	0.47	54.8	1.823
	Heptane[1]	2.04	0.54	45.0	
	Heptane	2.26	0.36	62.8	0.226
	Methanol[1]	5.45	0.63	11.0	
	Methanol	4.19	0.64	8.38	0.411
PIM-7	Toluene	3.88	0.69	29.0	0.191
	Acetone	3.05	0.58	45.5	0.148
	Heptane	3.22	0.41	19.6	1.838
	Methanol	4.94	0.79	13.0	0.301
PIM-8	Toluene	3.45	0.74	30.9	0.098
	Acetone	4.07	0.71	27.3	0.068
	Methanol	5.53	0.74	13.8	0.058
	Heptane	2.52	0.58	51.1	0.051

[1] Obtained from [34]

It can be seen in Table 1 that there is fairly good agreement between the monolayer sorption capacity, v_m, of PIM-1 obtained within this study and that reported previously. Differences in the mono and higher layer adsorption parameters, h and f, can be seen for toluene and heptane in PIM-1, whereas the parameters for methanol are similar. Larger values of the energetic parameter for the higher adsorption layer, f, typically leads to convexity within the isotherm at higher activity values, *as seen in Fig. 3*. In the case of methanol, low h and high f values indicate the formation of a monolayer within the PIM is unfavourable (although the capacity is relatively large), whilst the formation of the upper layers is somewhat favourable. This implies clustering phenomena of methanol within the PIM matrix, *indicating* interactions between methanol and PIM are weak, so that methanol acts as a non-solvent.

It was found for the PIM-7 and PIM-8 that the monolayer adsorption capacity was higher for all the solvents tested compared to PIM-1. Higher values of the upper layer energetic parameter, f, for toluene in PIM-7 and PIM-8 may indicate these polymers are more susceptible to swelling in this solvent compared to the PIM-1, although this was counterbalanced by a lower h value that could imply weaker interactions due to unfavourable monolayer formation. The discrepancy between our work and [34] over the exponential uptake relationship that occurs at higher vapour activity into PIM-1 may be due to capillary condensation into mesoporous regions of the PIM-1 resulting from different processing histories. This analysis verifies the porous nature of these three polymers, and suggests that some differences in the OSN performance should be expected.

3.2 Characterisation of the support membranes

Optimisation was conducted on the phase inversion parameters in attempts to fabricate support membranes with similar pore sizes and distributions, enabling *a fair* comparison between the two final composite membranes. To avoid additional complications with the coating process, it was desirable to avoid the use of preservatives within the support membranes. Consistent across the PAN membranes was that drying from a solvent with lower surface tension helped prevent pore collapse *whilst maintaining* a smoother membrane surface, Supplementary Information, Sections S4 and S5. Similar results have been observed for polysulfone membranes [35]. Decreasing the casting speed of the PAN membranes led to membranes with larger pore size, and with an apparent decrease in the number of surface pores as characterised by AFM (Supplementary Information, Section S5).

The two polymer support membranes that were used for the roll-to-roll coating line of the PIMs displayed similar pore sizes in the range of 20 - 25 nm, as shown in Fig. 4a. Crosslinking of the Ultem 1000 support led to a detectable change in the pore size, along with a slight broadening of its distribution, but the membrane remained flexible in the dry state, and did not suffer from brittleness.

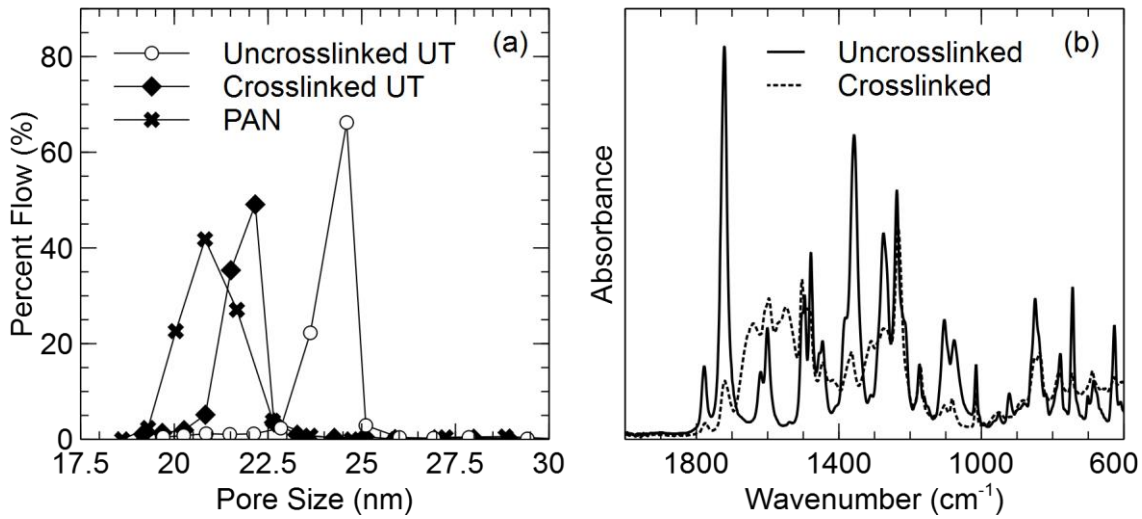

Fig. 4. (a) Pore sizes of the support membranes used for the PIM coatings and (b) the ATR-FTIR spectrum of Ultem 1000 before and after the crosslinking process.

ATR-FTIR was measured to assess the influence of the crosslinking on the x-UT support membrane, Fig. 4b. On the uncrosslinked UT, a major band can be seen at 1722 cm^{-1}, attributable to the symmetric C=O stretching (imide). This band decreases as the imide transforms into an amide, creating new bands at 1650 cm^{-1} and 1540 cm^{-1} that can be attributed to N-H stretching (amide) and C=O stretching (amide), respectively.

Imaging was further conducted on the support membranes to assess the structure and surface morphologies. Typical images are shown in Fig. 5, with further AFM images and characterisation shown in the Supplementary Information, Section S5. Capillary flow porometry suggests that the pore size of the support membranes is similar, while the AFM images suggest there is a significant difference in the morphology of the surface structure. It can be seen that both support membranes have a sponge structure, with an apparent skin layer. The PAN membrane appears to have a smoother surface with more uniform pore distribution. The x-UT membrane appears less uniform, and it seems likely that this is influenced by the chemical crosslinking procedure.

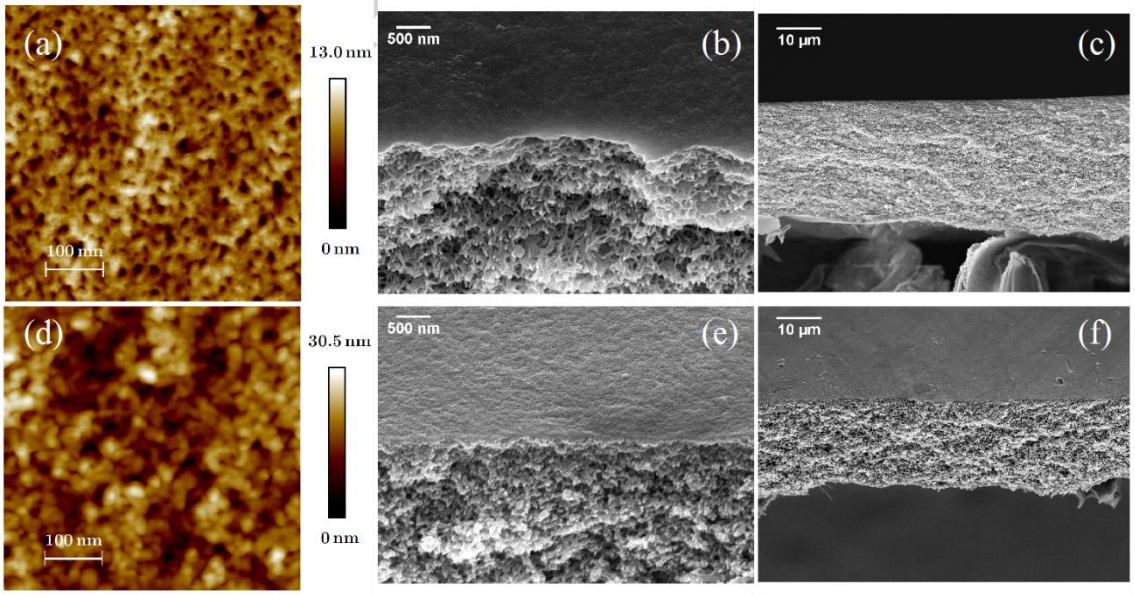

Fig. 5. Top row: (a) 500x500 nm AFM scan, and (b) and (c) cross section SEM images of PAN membrane, and bottom row: (d) 500x500 nm AFM scan, and (e) and (f) cross section SEM images of x-UT membrane, that were characteristic of the support membranes used for the coating trials.

3.3 Composite membrane fabrication and analysis

PIM coatings were conducted via pilot line roll-to-roll dip coating on to the support membranes described previously. For the PAN membrane, the lower pore size variant (with 30 seconds of evaporation prior to phase inversion) appeared to produce better coatings. This was based upon observations from optical microscopy of preliminary coatings of two different pore sized PAN membranes that are shown within Supplementary Information, Section S6.

3.3.1 Formation and assessment of the coated PIM layer

Scanning Electron Microscopy (SEM) was used to assess the thickness of the coating layer after fabrication on the roll-to-roll coating process. Dip coating in itself is a well-established process for thin film manufacture, however, fundamental understanding of the process is challenging due to the time-dependent nature of viscosity, concentration, and surface tension driven gradients that occur immediately after withdrawal from the coating bath. For a withdrawal speed above ~0.6 m min^{-1}, the coating thickness is dominated by the balance of viscous drag to gravitational , captured by the following correlation [36]:

$$\boldsymbol{h_0 = 0.8\left(\frac{\eta V}{\rho g}\right)^{1/2}} \quad (3)$$

where h_o is the wet film thickness, η is the viscosity, V is the withdrawal speed, ρ is the density of coating solution, and g is the gravitation force. The Landau-Levich equation can be used to estimate the wet film thickness resulting from dip coating using Newtonian fluids when the withdrawal speed is below ~0.6 m min^{-1}, and the coating solution is low viscosity. In this case, surface tension forces become more relevant to the coating phenomena, and the empirically derived equation dictating the final film thickness is given by [36]:

$$\boldsymbol{h_1 = 0.94\left(\frac{(\eta V)^{2/3}}{\gamma_{L,V}^{1/6}(\rho g)^{1/2}}\right)} \quad (4)$$

where γ_{LV} is the liquid-vapour surface tension. Multiplying the predicted wet thickness by the solids concentration in the coating solution gave rise to the estimated *thicknesses* listed in Table 2. The extremely low viscosities of these dilute PIM solutions *suggests it is likely that the film thickness will fall between those estimated from Equations (3) and (4), even though the speed is >0.6 m min^{-1} in all cases.*

Table 2. Details of PIM coatings applied *along with predicted and observed thicknesses*.

Coat no.	Polymer	Wt % (w/w)	Withdrawal Speed, V	Estimated h_o (nm)	Estimated h_1 (nm)	Observed thickness (nm)
1	PIM-1	0.6	5 m min^{-1}	390	160	200 - 300
2	PIM-7	1	5 m min^{-1}	670	270	600 - 800
3	PIM-7	0.6	1 m min^{-1}	189	56	100 - 200
4	PIM-7	0.6	5 m min^{-1}	390	160	200 - 300
5	PIM-8	0.6	5 m min^{-1}	390	160	200 - 300

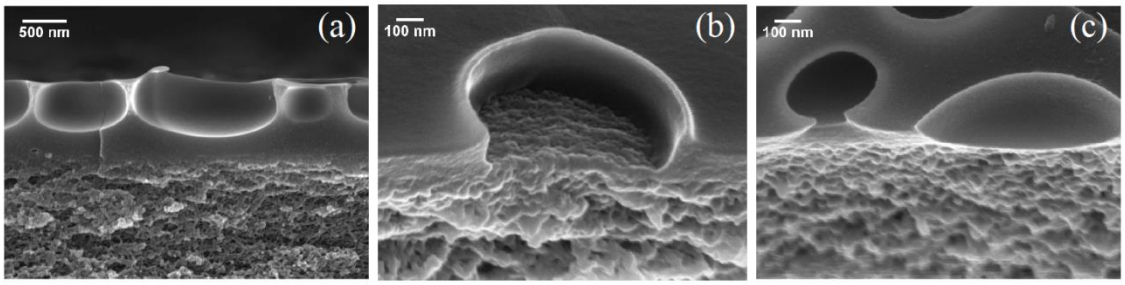

Fig. 6. Cross section SEM images of PIM-7 coated PAN membranes using $CHCl_3$/EtOH coating solution at a PIM concentrations of (a): 1 wt %, and (b) and (c): 0.6 wt %. Line speeds of the coating trials were at (a) 5 m min^{-1}, (b) 1 m min^{-1}, and (c) 5 m min^{-1}.

Coating on to porous substrates using volatile solvents presents a number of issues including popping, cratering, outgassing, and pinholes, which can result in similar irregular features in the final coated film, making it challenging to distinguish the root cause [37]. Preliminary coating trials were conducted in an attempt to find a stable coating regime. It can be seen in Fig. 6 that the formation of craters was a common occurrence during the coating trials. It is apparent that the occurrence of these defects did not arise definitively from our efforts to fabricate thin layers from a lower polymer concentration. As seen from Fig. 6a, in the case of coating from a higher polymer concentration, the craters did not extend down to the surface of the support membrane, suggesting that these bubble like voids are not solely due to surface tension driven defects. *However, comparing Fig. 6b and Fig. 6c, and as expected from Equation (4),* the surface tension effect *may be more* relevant at a lower coating speed *and for thinner layers*. *In this instance,* it can be seen that in the case of a low coating speed, Fig. 6b, the PIM layer has dewetted, as one can see the surface of the ultrafiltration support membrane. At a higher speed, when the surface tension effect should be less relevant, the surface of the ultrafiltration support membrane cannot be seen through the bubble-like voids. The goal of our research is to investigate the effect of manipulated changes to the PIM molecular structure on the performance of composite membranes. For any fair comparison, it is imperative that the coating layer be as uniform as possible with a consistent support membrane. Based upon these preliminary trials, it was decided to fix the polymer concentration at 0.6 wt % with a web speed of 5 m min^{-1}, and focus on the effects of the coating solution composition and the choice of support membrane on the final composite membrane fabrication and performance.

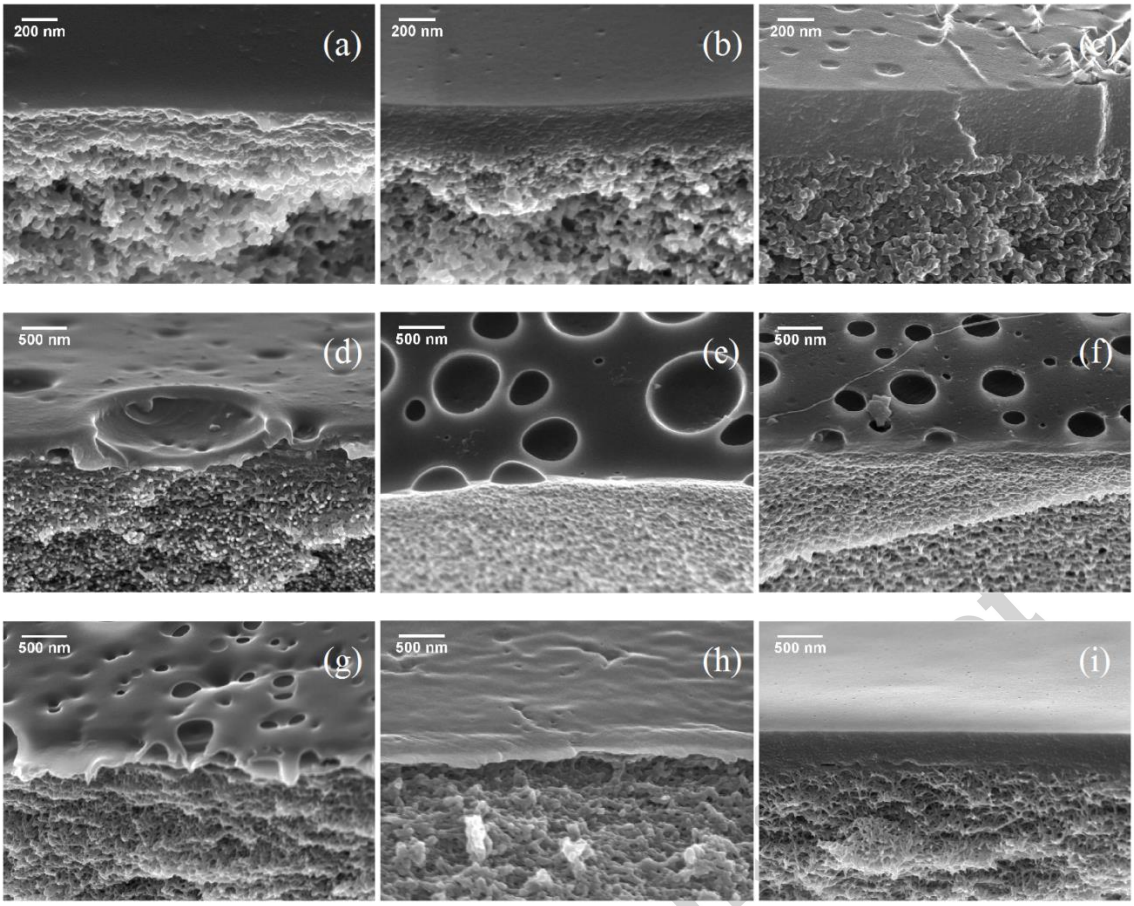

Fig. 7. Cross Section SEM images of (a) PIM-1, (b) PIM-7, and (c) PIM-8 coated on to x-UT substrate, (d) PIM-1, (e) PIM-7, and (f) PIM-8 coated on to PAN from a solution of $CHCl_3$ (1.0 wt % EtOH additive), and (g) PIM-1, (h) PIM-7, and (i) PIM-8 coated on to PAN from a solution of $CHCl_3$ (1.0 wt % MeOH additive). For all coatings the web speed was constant at 5 m min^{-1} and a polymer concentration of 0.6 wt % was used throughout.

Cross sectional SEM images are shown in Fig. 7 for a broader study on the *coating feasibility* of these three different PIMs. In all cases the thickness of the PIM layer is <500 nm. It can be seen that under certain conditions uniform films were obtainable. The top row of Fig. 7 shows that more uniform films were obtainable on the x-UT substrate without the need to adjust the composition of the coating solution. It can be seen in Fig. 7b and Fig. 7c that the PIM films show early signs of crater formation, but the diameter of these craters is <100 nm and *they do not appear to penetrate deeply enough into the film to create pinholes in the separation layer*. The diameter of the craters on the PAN support when coated under identical conditions is much larger, upwards of 500 nm, as shown in Fig. 7e and Fig. 7f. For the PAN substrate, when using methanol as the co-solvent for the PIM-7 and PIM-8, the resulting coated films were substantially more uniform than those obtained with ethanol. Light microscope images are presented in the Supplementary Information, Section S7. In all cases, the surface energy of the support membrane is higher than the surface tension of the coating solution (chloroform), and so the coating conditions should be favourable.

In many cases the surface depressions were not seen to influence the performance of the membrane; the separation properties of the PIM-1 were consistent across both supports, as well as being similar to those reported elsewhere in the literature [11,38,39]. It is desirable from the manufacturability viewpoint that the coatings are as uniform as possible to ensure reproducibility of fabrication.

3.3.2 Performance testing of composite PIM membranes in OSN

3.3.2.1 PIM-1.

The PIM-1 composite membranes on PAN supports exhibited higher permanence than those on the x-UT support *for all solvents tested*. Vapour sorption analysis suggested that the monolayer sorption capacity, v_m, from the GAB model of the PIM-1 was similar in toluene and heptane, with values of 2.31 and 2.26 mmol g^{-1} respectively. When tested in crossflow filtration with either of these solvents using polystyrene standards as marker solutes, a MWCO of 500 – 800 g mol^{-1}, across either of the support membranes *was obtained*. The composite membranes were seen to undergo some minor compaction, Fig. S13, with a corresponding change in MWCO. All experiments were *further* conducted at 30 bar TMP. It can be seen from AFM in Fig. 5 that the surface of the PAN appears to have a much higher density of pores than that of the x-UT, which may lower the mass transfer resistance from the support membrane, *giving rise to the higher permeance*. As seen previously, however, this may have incurred complications with regards to the dip coating process and assisted in the crater formation.

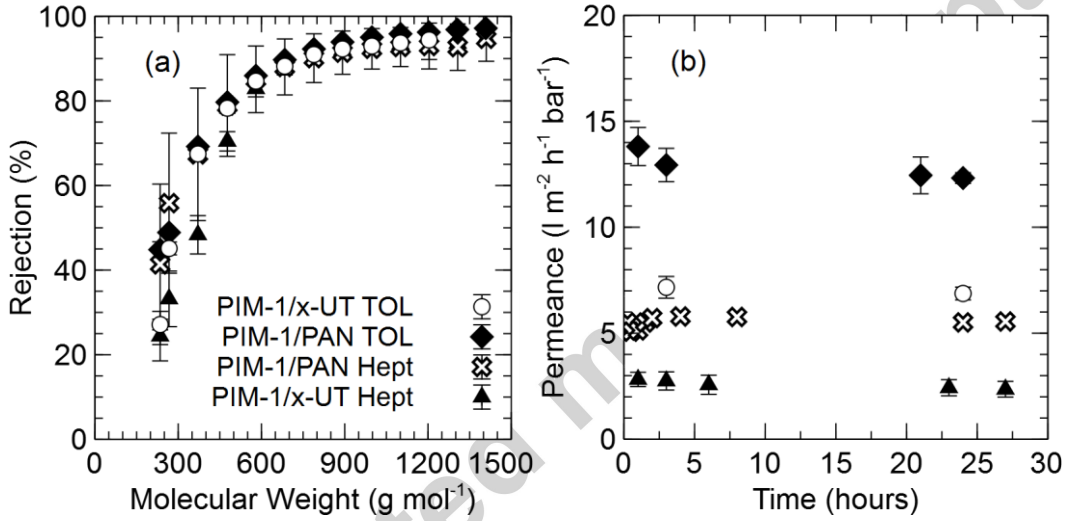

Fig. 8. MWCO (a) and permeance (b) graphs of PIM-1 coated on to x-UT or PAN support membranes with 1 g l^{-1} polystyrene marker solutes in either heptane or toluene as solvent. 30 bar TMP, 30°C, 1 L min^{-1} flowrate.

Further screening was conducted on PIM-1/x-UT membranes in three additional solvents over three days of continuous crossflow filtration, as shown in Fig. 9, with polystyrene standards as marker solutes. It became apparent that after some preliminary compaction during the first day, the membrane performance was stable. The MWCO of the PIM-1/x-UT in these five solvents, *except methanol*, is around 500 - 800 g mol^{-1}, and is similar to that reported previously [11,38,39]. Acetonitrile is a widely used solvent within the pharmaceutical industry, and its absence from published data on Organic Solvent Nanofiltration prompted a screening study to recently be conducted for various OSN membranes [40]. The PIM-1/x-UT membrane can be considered stable in MeCN (where the PAN fails), and displayed consistent performance over a few days testing, with promising separation properties.

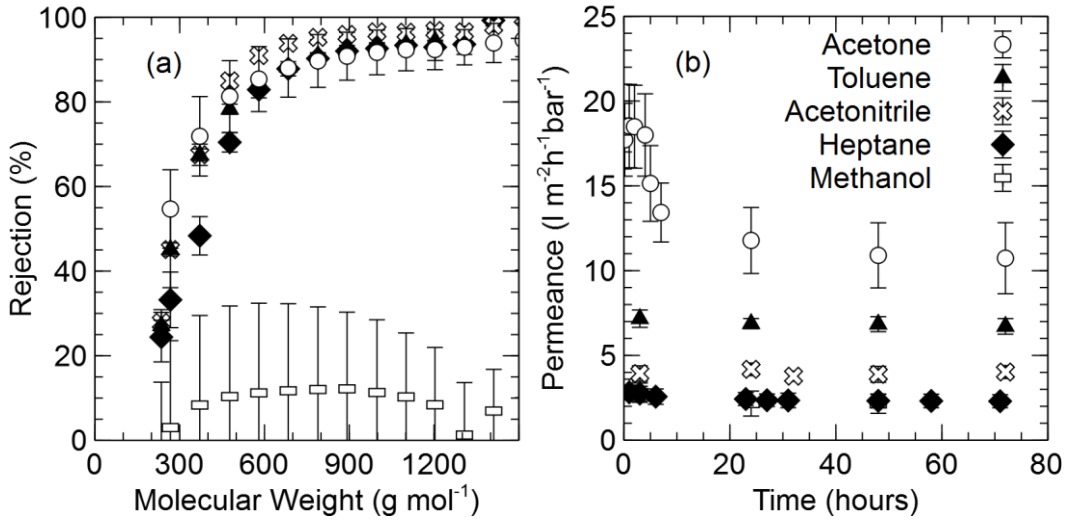

Fig. 9. MWCO (a) and permeance time plot (b) of PIM-1/x-UT membranes with polystyrene as marker solutes in five different solvents over 3 days of testing at 30 bar TMP, 30°C, 1 L min^{-1}.

No detachment of the PIM-1 layer was observed during filtration with acetone, although the OSN performance may be compromised at such high permeance due to concentration polarisation phenomena. High acetone permeance has been reported previously on a PAN support [11], prompting the authors of that study to crosslink an epoxy resin inside the PIM-1. This lowered the performance of the PIM-1 in alkanes, making them unsuitable for aliphatic solvents, *as reported by the authors*. As seen from Fig. 10, the pure solvent permeances of the PIM-1 appear to be correlated with the Hansen Solubility Parameter of the solvent. A similar dependency of the flux on the solubility parameter of the solvent has been reported for PDMS based membranes [41], although the solubility and swelling phenomena of PDMS is *understood to a greater extent*. It can be expected that crosslinking other chemicals inside the PIM-1 will shift the apparent solubility parameter of the polymer film, possibly lowering the performance in certain solvents depending upon the *direction of the* shift. It can also be seen in Fig. 9 that the influence of the solubility parameter has hampered the performance of the membrane in methanol when polystyrenes are used as marker solutes. Analysis with the GAB model verified that the methanol has weak interactions with the PIM polymer.

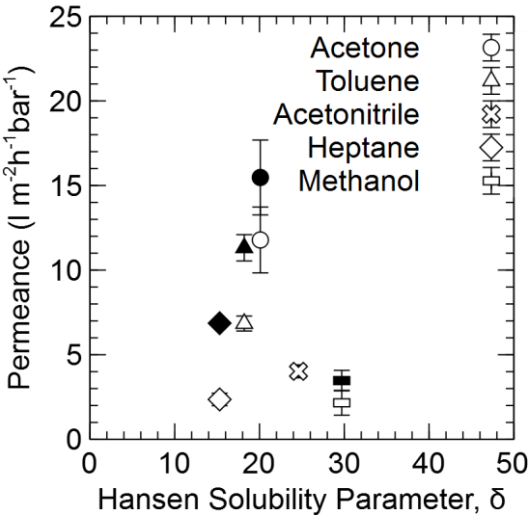

Fig. 10. Solvent permeance plotted against total Hansen Solubility Parameter for PIM-1 composite membranes. Test conditions of 30 bar TMP, 30°C, 1 L min^{-1} with values taken after a minimum of 24 hours permeation. Black markers represent data for PAN support, whilst white are for x-UT support membrane.

3.3.2.2 PIM-7 and PIM-8

When comparing between the PIM-1, PIM-7, and PIM-8, the most optimised membranes were chosen for comparison. In these, the coating conditions enabled the PS rejection to tend towards 100%. Fig. 11 shows the comparison of the three different PIMs coated on the PAN support membrane. The cross sectional *images* of the *PIM-1, PIM-7, and PIM-8 composite membranes are from Fig. 7d, Fig. 6a, and Fig. 7f, respectively.* The steady state permeances are also noted on the figure. The rejection properties of the membranes are very similar, and the discrepancy in permeance and rejection likely arises from variances in both the support, and in the coating layer. *It can be concluded that there is insufficient evidence to suggest the separation properties of these three PIMs are significantly different when testing the OSN performance with polystyrene marker solutes*. *Therefore, further OSN characterisation was conducted with alternative marker solutes*.

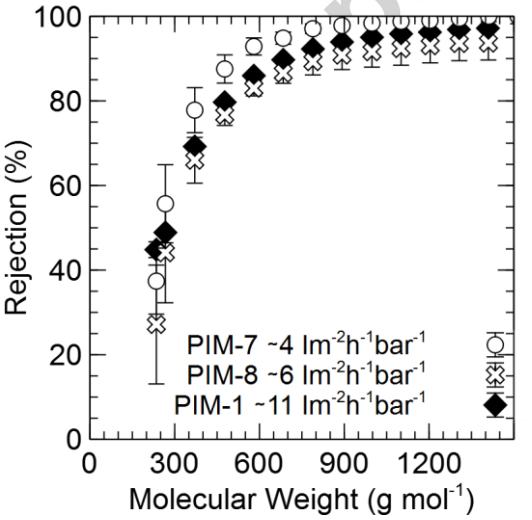

Fig. 11. Comparison between PIM-1, PIM-7, and PIM-8 composite membranes on PAN in toluene with polystyrene marker solutes at 30 bar TMP, 30°C, 1 L min^{-1} flowrate.

3.3.2.3 Performance in branched and straight alkanes

To further study the efficacy of the PIMs separating ability, filtrations were *conducted* with two isomeric hexadecane *(226 g mol^{-1})* species. *It is now convenient to introduce a separation factor*, *α*, between these straight and branched alkane, defined as:

$$\alpha = \frac{1-R_{n-C_{16}}}{1-R_{i-C_{16}}} \quad (5)$$

where R is the membrane rejection as defined previously. *Fig. 12* shows that the *separation factor* is a function of the membrane permeance *in certain cases*, with rejection data tabulated in Supplementary Information, Section S9. The low permeance of this PIM-7 membrane is a result of testing a thicker membrane (Fig. 6a). It can be seen that the separation properties of the PIM-1 and PIM-7 are very similar, and that these two PIMs do not perform as well as the PIM-8 in this model alkane system, *which was found to exhibit a higher separation factor between the hexadecane isomers*.

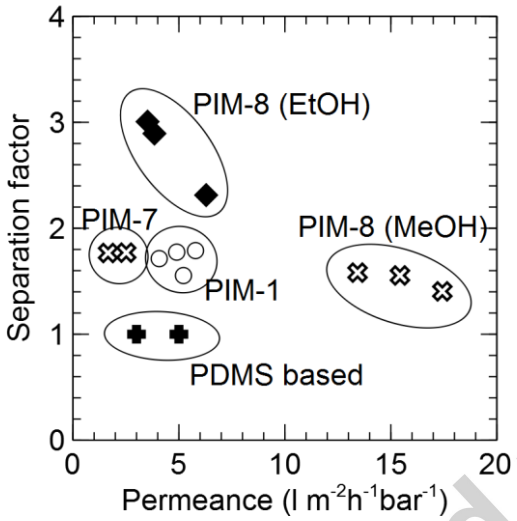

Fig. 12. Separation factor of *n*-C_{16} over *i*-C_{16} as a function of membrane permeance for two different coatings of PIM-8 and a PIM-1 membrane. All coatings are conducted on PAN membrane. 30 bar TMP, 30°C, 1 L min^{-1} flowrate.

On switching from heptane to toluene, the aromatic stability of the three different PIMs can be further studied by obtaining the permeability coefficient of each specie within the mixture. For this purpose, the solution diffusion model is adequate for analysis of the transport mechanism [42], given by:

$$J_i = P_i \left[c_{io} - c_{ip} \exp\left(\frac{-V_i \Delta P}{RT}\right)\right] \quad (6)$$

where J_i is the membrane flux for component i (mol m^{-2} h^{-1}), P_i is the permeability coefficient for component i (mol m^{-2} h^{-1}), c_{io} and c_{ip} are feed and permeate side concentrations of component i respectively (mol fraction), V_i is the molar volume of component i (m^3 mol^{-1}), ΔP is the Trans Membrane Pressure (bar), R is the gas constant (m^3 bar K^{-1} mol^{-1}), and T is the temperature (K). The concentrations of each species present in the filtration mixture were obtained from the GC-FID, and the permeability coefficients were calculated. The data is summarised in *Supplementary Information, Table S2,* and a *normalised* permeability coefficient, $P_i/P_{i-C_{16}}$, is introduced to allow for comparative behavior between the different PIMs owing to the different membrane thicknesses. It can be seen that the permeability coefficient of the solvent relative to the branched alkane remains

an order of magnitude higher when switching from toluene to heptane. The permeability coefficient of the straight chain molecule, however, decreases relative to the branched alkane, causing a decrease in the *separation factor*. After switching the solvent from heptane to toluene, a further switch back to heptane was made. The heptane permeance of the membranes was significantly higher after filtration with an aromatic solvent. The membranes were removed from the filtration cells, immersed overnight in methanol, and allowed to dry before returning to filtration with heptane. After this methanol treatment, the performance of PIM membranes returned close to their original values. The permeability coefficients of each of the species during this testing period are displayed in the Supplementary Information, Table S2. The solvent permeance is plotted over the filtration time in Fig. 13. In line with research conducted on thick films of PIM-1, the methanol treatment appeared to eradicate the past processing history, decreasing the permeability coefficients of both solvent and solutes by more than a factor of 2. As a result, the *separation factor* also improved after the methanol treatment.

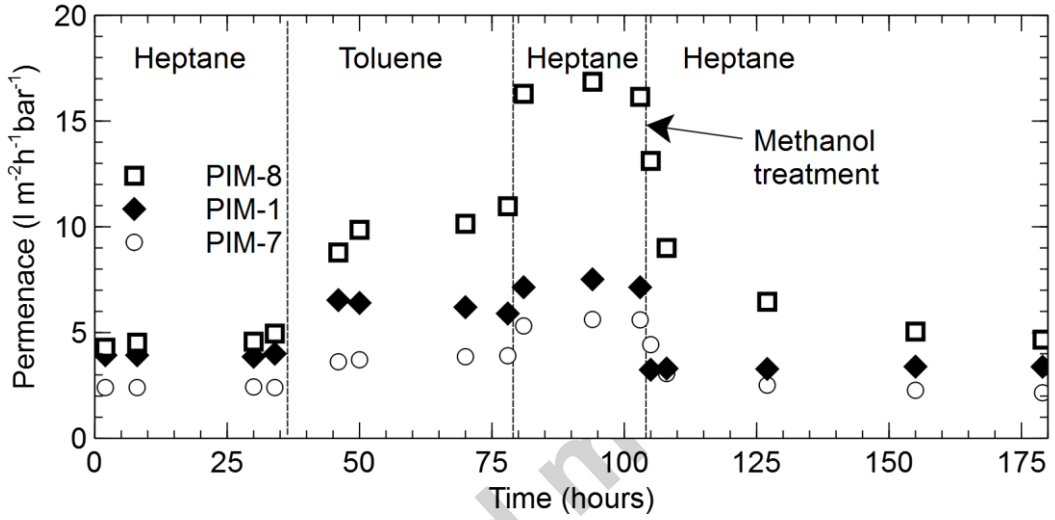

Fig. 13. Long term permeance data of the three different PIM membranes coated on PAN when tested in n and i C_{16} solutes at 0.5 wt % concentration each. 30 bar TMP, 30°C, 1 L min^{-1}. The solvents were cycled from heptane to toluene, back to heptane, and continuation in heptane after methanol treatment.

Our research efforts to eliminate the cratering effect observed for PIM-8 apparently led to a more open membrane structure via the use of methanol in the coating solution. It is known that PIM-1 is significantly affected by processing history, and that free volume can be restored or modified by solvent treatment. Fabricating PIM-1 from THF or $CHCl_3$ also leads to different membrane performance. *The performance data suggests* that PIM-8 membranes with distinctly different pore sizes were produced by using either methanol or ethanol respectively in the coating solution with chloroform. In this instance after casting, methanol treatment did not substantially change the filtration performance after toluene filtration. It is thus apparent that the resulting microstructure of the finally obtained PIM is highly sensitive to the coating and drying conditions, and remains important irrespective of solvent plasticisation phenomena. These findings are consistent with those reported during the development of a glassy polyimide membranes: that is, as the membranes becomes tighter, they become more selective [43].

A minor tweak in the coating solution of the PIM-8 polymer yielded a membrane with a more open structure, and subsequently lower selectivity. Given that such a subtle change exerted a significant effect on the membrane performance, the membrane design is made

more complicated. It becomes challenging to assess the potential a novel polymer has in fulfilling its intended use based solely upon the measurable properties of the polymer. PDMS based membranes in the rubbery state exhibit almost no *separation factor* between alkane isomers, with the rejection either being above or below that of the PIM variants. The plasticization behavior of the PIM-1 is a complex phenomenon [44], and the extent to which the polymer backbone is in a static or dynamic state during solvent permeation is unknown. The *separation factor* of straight over branched molecules, however, is a clear sign that some regions of the polymer backbone are either preventing or hindering the transport of the branched molecule, whilst enabling that of a straight chain counterpart.

4 Conclusions

A series of PIM composite membranes were prepared on two different support membranes under various conditions. All PIMs were found to yield higher quality coatings on a crosslinked Ultem 1000 support membrane with less optimization than was required for a PAN support. This conclusion was consistent across PAN membranes of different pore sizes, both below and above that of the x-UT support. The coated PIM on the x-UT substrate exhibited less tendency to form craters than identical coatings conducted on PAN. With the ability to remain flexible in the dry state, the crosslinked Ultem 1000 can thus be considered an attractive support membrane for OSN applications. The solvent permeance of the composite membranes decreased during the first day of testing, characteristic of compaction phenomena that is observed with other OSN membranes, and subsequently appeared stable over a few days of continuous filtration. PIM-8 was found to have a higher *separation factor* between a straight and branched chain C_{16} alkanes compared to PIM-1 and PIM-7, verifying a previous observation that this polymer has a stronger bias towards sub-nanometer pores. Branched and straight separations have been of interest to membrane researchers, and these results show untapped potential exists in this area. Methanol treatment of the composite membrane was shown to somewhat eradicate the past solvent filtration history, restoring the permeability coefficients of the test species close to their original values.

5 Acknowledgments

The authors wish to acknowledge Shell and the EPSRC for funding a CASE award for M.C (EP/L50547X/1). The authors also wish to acknowledge Adam Marsh for assistance with the GPC analysis.

References

[1] N.B. McKeown, Polymers of Intrinsic Microporosity, ISRN Mater. Sci. (2012) 1–16.

[2] M. Galizia, W.S. Chi, Z.P. Smith, T.C. Merkel, R.W. Baker, B.D. Freeman, 50th Anniversary Perspective : Polymers and Mixed Matrix Membranes for Gas and Vapor Separation: A Review and Prospective Opportunities, Macromolecules. 50 (2017) 7809–7843.

[3] M.L. Jue, D.Y. Koh, B.A. McCool, R.P. Lively, Enabling widespread use of microporous materials for challenging organic solvent separations, Chem. Mater. 29 (2017) 9863–9876.

[4] H.R. Kricheldorf, N. Lomadze, D. Fritsch, G. Schwarz, Cyclic and Telechelic Ladder Polymers Derived from Tetrahydroxytetramethylspirobisindane and 1,4-

Dicyanotetrafluorobenzene, J. Polym. Sci. Part A Polym. Chem. 44 (2006) 5344–5352.

[5] J. Song, N. Du, Y. Dai, G.P. Robertson, M.D. Guiver, S. Thomas, I. Pinnau, Linear High Molecular Weight Ladder Polymers by Optimized Polycondensation of Tetrahydroxytetramethylspirobisindane and 1,4-Dicyanotetrafluorobenzene, Macromolecules. 41 (2008) 7411–7417.

[6] D. Naiying, S. Jingshe, G.P. Robertson, I. Pinnau, M.D. Guiver, Linear high molecular weight ladder polymer via fast polycondensation of 5,5',6,6'-tetrahydroxy- 3,3,3',3'-tetramethylspirobisindane with 1,4-dicyanotetrafluorobenzene, Macromol. Rapid Commun. 29 (2008) 783–788.

[7] N.B. McKeown, The synthesis of polymers of intrinsic microporosity (PIMs), Sci. China Chem. 60 (2017) 1023–1032.

[8] J. Zhang, J. Jin, R. Cooney, S. Zhang, Synthesis of polymers of intrinsic microporosity using an AB-type monomer, Polymer. 57 (2015) 45–50.

[9] L. Gao, M. Alberto, P. Gorgojo, G. Szekely, P.M. Budd, High-flux PIM-1/PVDF thin film composite membranes for 1-butanol/water pervaporation, J. Memb. Sci. 529 (2017) 207–214.

[10] K. Heinrich, Polymere mit intrinsischer Mikroporosität - Membranmaterialien mit Zukunft?, Tech. Fak. (2009).

[11] D. Fritsch, P. Merten, K. Heinrich, M. Lazar, M. Priske, High performance organic solvent nanofiltration membranes: Development and thorough testing of thin film composite membranes made of polymers of intrinsic microporosity (PIMs), J. Memb. Sci. 401-402 (2012) 222–231.

[12] H. Shamsipur, B.A. Dawood, P.M. Budd, P. Bernardo, G. Clarizia, J.C. Jansen, Thermally rearrangeable PIM-polyimides for gas separation membranes, Macromolecules. 47 (2014) 5595–5606.

[13] B.S. Ghanem, N.B. McKeown, P.M. Budd, D. Fritsch, Polymers of Intrinsic Microporosity Derived from Bis(phenazyl) Monomers, Macromolecules. 41 (2008) 1640–1646.

[14] B. Ghanem, F. Alghunaimi, N. Alaslai, X. Ma, I. Pinnau, A. Volkov, J. Jin, N.B. McKeown, N.B. McKeown, A. Walton, N.B. McKeown, New phenazine-containing ladder polymer of intrinsic microporosity from a spirobisindane-based AB-type monomer, RSC Adv. 6 (2016) 79625–79630.

[15] Y. Rogan, L. Starannikova, V. Ryzhikh, Y. Yampolskii, P. Bernardo, F. Bazzarelli, J.C. Jansen, N.B. McKeown, Synthesis and gas permeation properties of novel spirobisindane-based polyimides of intrinsic microporosity, Polym. Chem. 4 (2013) 3813–3820.

[16] W.F. Yong, Z.K. Lee, T.-S. Chung, M. Weber, C. Staudt, C. Maletzko, Blends of a Polymer of Intrinsic Microporosity and Partially Sulfonated Polyphenylenesulfone for Gas Separation, ChemSusChem. 9 (2016) 1953–1962.

[17] M.M. Khan, G. Bengtson, S. Neumann, M.M. Rahman, V. Abetz, Synthesis, characterization and gas permeation properties of anthracene maleimide-based polymers of intrinsic microporosity, RSC Adv. 4 (2014) 32148–32160.

[18] D. Fritsch, G. Bengtson, M. Carta, N.B. McKeown, Synthesis and Gas Permeation Properties of Spirobischromane-Based Polymers of Intrinsic Microporosity, Macromol. Chem. Phys. 212 (2011) 1137–1146.

[19] N. Du, G.P. Robertson, I. Pinnau, S. Thomas, M.D. Guiver, Copolymers of Intrinsic Microporosity Based on 2,2',3,3'-Tetrahydroxy-1,1'-dinaphthyl., Macromol. Rapid Commun. 30 (2009) 584–588.

[20] J. Zhang, J. Jin, R. Cooney, Q. Fu, G.G. Qiao, S. Thomas, T.C. Merkel, Synthesis of perfectly alternating copolymers for polymers of intrinsic microporosity, Polym. Chem. 6 (2015) 5003–5008.

[21] F.Y. Li, Y. Xiao, T.-S. Chung, S. Kawi, High-Performance Thermally Self-Cross-Linked Polymer of Intrinsic Microporosity (PIM-1) Membranes for Energy Development, Macromolecules. 45 (2012) 1427–1437.

[22] Q. Song, S. Cao, R.H. Pritchard, B. Ghalei, S.A. Al-Muhtaseb, E.M. Terentjev, A.K. Cheetham, E. Sivaniah, Controlled thermal oxidative crosslinking of polymers of intrinsic microporosity towards tunable molecular sieve membranes., Nat. Commun. 5 (2014) 4813.
[23] P. Salehian, W.F. Yong, T.-S. Chung, Development of high performance carboxylated PIM-1/P84 blend membranes for pervaporation dehydration of isopropanol and CO2/CH4 separation, J. Memb. Sci. 518 (2016) 110–119.
[24] N. Du, M.M.D.- Cin, I. Pinnau, A. Nicalek, G.P. Robertson, M.D. Guiver, Azide-based cross-linking of polymers of intrinsic microporosity (PIMs) for condensable gas separation., Macromol. Rapid Commun. 32 (2011) 631–6.
[25] M.M. Khan, G. Bengtson, S. Shishatskiy, B.N. Gacal, M.M. Rahman, S. Neumann, V. Filiz, V. Abetz, Cross-linking of Polymer of Intrinsic Microporosity (PIM-1) via nitrene reaction and its effect on gas transport property, Eur. Polym. J. 49 (2013) 4157–4166.
[26] F.Y. Li, Y. Xiao, Y.K. Ong, T.-S. Chung, UV-Rearranged PIM-1 Polymeric Membranes for Advanced Hydrogen Purification and Production, Adv. Energy Mater. 2 (2012) 1456–1466.
[27] F.Y. Li, T.-S. Chung, Physical aging, high temperature and water vapor permeation studies of UV-rearranged PIM-1 membranes for advanced hydrogen purification and production, Int. J. Hydrogen Energy. 38 (2013) 9786–9793.
[28] Q. Song, S. Cao, P. Zavala-Rivera, L.P. Lu, W. Li, Y. Ji, S.A. Al-Muhtaseb, A.K. Cheetham, E. Sivaniah, Photo-oxidative enhancement of polymeric molecular sieve membranes., Nat. Commun. 4 (2013) 1918.
[29] R.W. Baker, B.T. Low, Gas Separation Membrane Materials: A Perspective, Macromolecules. 47 (2014) 6999–7013.
[30] B. Jung, J.K. Yoon, B. Kim, H.-W. Rhee, Effect of crystallization and annealing on polyacrylonitrile membranes for ultrafiltration, J. Memb. Sci. 246 (2005) 67–76.
[31] J. da Silva Burgal, L.G. Peeva, S. Kumbharkar, A. Livingston, Organic solvent resistant poly(ether-ether-ketone) nanofiltration membranes, J. Memb. Sci. 479 (2015) 105–116.
[32] Y.H. See Toh, X.X. Loh, K. Li, A. Bismarck, A.G. Livingston, In search of a standard method for the characterisation of organic solvent nanofiltration membranes, J. Memb. Sci. 291 (2007) 120–125.
[33] M.L. Jue, C.S. McKay, B.A. McCool, M.G. Finn, R.P. Lively, Effect of Nonsolvent Treatments on the Microstructure of PIM-1, Macromolecules. 48 (2015) 5780–5790.
[34] O. Vopička, K. Friess, V. Hynek, P. Sysel, M. Zgažar, M. Šípek, K. Pilnáček, M. Lanč, J.C. Jansen, C.R. Mason, P.M. Budd, Equilibrium and transient sorption of vapours and gases in the polymer of intrinsic microporosity PIM-1, J. Memb. Sci. 434 (2013) 148–160.
[35] H.C. Park, Y.S. Moon, H.W. Rhee, J. Won, Y.S. Kang, U.Y. Kim, Effect of Solvent Exchange on the Morphology of Asymmetric Membranes, in: Membr. Form. Modif., 1999: pp. 110–124.
[36] C.J. Brinker, Dip Coating, in: Chemical Solution Deposition of Functional Oxide Thin Films, 2013.
[37] E.B. Gutoff, E.D. Cohen, Coating and Drying Defects: Troubleshooting Operating Problems, John Wiley & Sons, Inc., New Jersey, 2006.
[38] P. Gorgojo, S. Karan, H.C. Wong, M.F. Jimenez-Solomon, J.T. Cabral, A.G. Livingston, Ultrathin Polymer Films with Intrinsic Microporosity: Anomalous Solvent Permeation and High Flux Membranes, Adv. Funct. Mater. 24 (2014) 4729–4737.
[39] M. Lazar, Silicone Based Membranes for Organic Solvent Nanofiltration, RWTH Aachen University, 2015.
[40] M. Bastin, K. Hendrix, I. Vankelecom, Solvent resistant nanofiltration for acetonitrile based feeds: A membrane screening, J. Memb. Sci. 536 (2017) 176–185.
[41] S. Zeidler, U. Kätzel, P. Kreis, Systematic investigation on the influence of solutes on the separation behavior of a PDMS membrane in organic solvent nanofiltration, J. Memb. Sci. 429 (2013) 295–303.

[42] P. Marchetti, A.G. Livingston, Predictive membrane transport models for Organic Solvent Nanofiltration: How complex do we need to be?, J. Memb. Sci. 476 (2014) 530–553.
[43] L.S. White, Transport properties of a polyimide solvent resistant nanofiltration membrane, J. Memb. Sci. 205 (2002) 191–202.
[44] W. Ogieglo, K. Rahimi, S.B. Rauer, B. Ghanem, X. Ma, I. Pinnau, M. Wessling, How Do Organic Vapors Swell Ultrathin Films of Polymer of Intrinsic Microporosity PIM-1?, J. Phys. Chem. B. 121 (2017) 7210–7220.

Highlights

- Thin film composite membranes of PIM-1, PIM-7, and PIM-8 prepared by roll-to-roll dip coating for Organic Solvent Nanofiltration
- PAN and a crosslinked Ultem 1000 were used as support membranes
- Competitive membrane performance was achieved in various test solvents